ADVANCES IN ATMOSPHERIC SCIENCES, VOL. 26, NO. 6, 2009, 1198–1208

Water Vapor, Cloud, and Surface Rainfall Budgets Associated with the Landfall of Typhoon Krosa (2007): A Two-Dimensional Cloud-Resolving Modeling Study

YUE Caijun*[1,2] (岳彩军), SHOU Shaowen[3] (寿绍文), and Xiaofan LI[4]

[1] *Shanghai Typhoon Institute, China Meteorological Administration, Shanghai* 200030

[2] *Laboratory of Typhoon Forecast Technique/China Meteorological Administration, Shanghai* 200030

[3] *School of Atmospheric Sciences, Nanjing University of Information Science and Technology, Nanjing* 210044

[4] *Joint Center for Satellite Data Assimilation and NOAA/NESDIS/Center for Satellite Applications and Research Camp Springs, Maryland, USA*

(Received 30 August 2008; revised 24 March 2009)

ABSTRACT

Water vapor, cloud, and surface rainfall budgets associated with the landfall of Typhoon Krosa on 6–8 October 2007 are analyzed based on a two-dimensional cloud-resolving model simulation. The model is integrated with imposed zonally-uniform vertical velocity, zonal wind, horizontal temperature, and vapor advection from NCEP/Global Data Assimilation System (GDAS) data. The simulation data that are validated with observations are examined to study physical causes associated with surface rainfall processes during the landfall. The time- and domain-mean analysis shows that when Krosa approached the eastern coast of China on 6 October, the water vapor convergence over land caused a local atmospheric moistening and a net condensation that further produced surface rainfall and an increase of cloud hydrometeor concentration. Meanwhile, latent heating was balanced by advective cooling and a local atmospheric warming. One day later, the enhancement of net condensation led to an increase of surface rainfall and a local atmospheric drying, while the water vapor convergence weakened as a result of the landfall-induced deprivation of water vapor flux. At the same time, the latent heating is mainly compensated the advective cooling. Further weakening of vapor convergence on 8 October enhanced the local atmospheric drying while the net condensation and associated surface rainfall was maintained. The latent heating is balanced by advective cooling and a local atmospheric cooling.

Key words: budget, cloud-resolving modeling, Typhoon Krosa

Citation: Yue, C. J., S. W. Shou, and X. F. Li, 2009: Water vapor, cloud, and surface rainfall budgets associated with the landfall of Typhoon Krosa (2007): A two-dimensional cloud-resolving modeling study. *Adv. Atmos. Sci.*, **26**(6), 1198–1208, doi: 10.1007/s00376-009-8135-2.

1. Introduction

During summertime, many typhoons originate from the tropical western Pacific and make landfall and bring torrential rainfall to the southeastern coast region of China. Torrential rainfall may cause significant economic loss. Thus, typhoon landfall-induced torrential rainfall and the associated physical processes has been one of the most important topics studied in recent decades (e.g., Tuleya and Kurihara, 1978; Bender et al., 1985; Elsberry and Marks, 1999; Elsberry, 2002; Colle, 2003; Chen et al., 2004; Ji et al., 2007; Yue, 2009).

Cloud-resolving models have been used to study convective systems and associated precipitation (e.g., Tao, 2003; Gao and Li, 2008). The simulations have been validated with observations in terms of atmospheric thermodynamic profiles, surface fluxes, and surface rain rate in the tropics during the Global Atmospheric Research Program Atlantic Tropical Exper-

*Corresponding author: YUE Caijun, yuecaijun2000@163.com

iment (GATE) (e.g., Xu and Randall, 1996; Grabowski et al., 1996), Tropical Ocean Global Atmosphere Coupled Ocean Atmosphere Response Experiment (TOGA COARE) (e.g., Wu et al., 1998; Li et al., 1999), Atmospheric Radiation Measurement (ARM) (e.g., Xu et al., 2002), and South China Sea Monsoon Experiment (SCSMEX) (e.g., Tao, 2003; Wang et al., 2007). Wang et al. (2007) and Xu et al. (2007) used a two-dimensional (2D) cloud-resolving model (the same model used in this study) to study rainfall processes during SCSMEX and during a separate torrential rainfall event in China, and validated these simulations with rain gauge and radar observations. The validated simulation data have been further applied to the analysis of surface rainfall budgets, which enhances understanding of water vapor and cloud processes associated with rainfall events during the life cycles of rainfall development.

Precipitation has not been analyzed in a proper framework in previous rainfall studies. The water vapor budgets (e.g., Gallus and Johnson, 1991; Tao and Simpson, 1993; Johnson et al., 2007) and apparent water vapor sinks (e.g., Caniaux et al., 1994) associated with precipitation have been examined to study convective development, using methods where precipitation is not an explicit item. The cloud budgets (e.g., Gamache and Houze, 1983; Chong and Hauser, 1989) have been investigated over convective and stratiform regions, where the transport of cloud hydrometeors links the two regions. However, the water vapor convergence and surface evaporation that are major water vapor sources for convective development and the production of precipitation are not included in the cloud budget. Gao et al. (2005a) combined the water vapor budget and cloud budget to derive a surface rainfall equation, where precipitation is determined by local water vapor storage, water vapor convergence, surface evaporation, and a cloud source/sink.

During the landfall of typhoons, the water vapor and large-scale dynamic conditions will be changed significantly due to different thermodynamic and dynamic capacities between the land and ocean. The question of rainfall evolution could hinge on how precipitation and clouds respond to the change of the large-scale forcing. In this study, a 2D cloud-resolving model simulation of a torrential rainfall event associated with the landfall of Typhoon Krosa (2007) over the eastern coast of China is conducted. The simulated rainfall is compared with rain gauge data, and the simulation data are further used to examine the rainfall and cloud responses to the large-scale forcing during the landfall with the analysis of water vapor, cloud, and heat budgets, as well as surface precipitation. In the next section, model and analysis methodologies are briefly described. In section 3, the history of Typhoon Krosa will be briefly described, and the simulated rain rate will be compared with observed rain gauge data. Then, the simulation data are used to conduct an investigation regarding the surface rainfall processes and associated cloud microphysical budgets. A summary is given in section 4.

2. Model and methodologies of analysis

The cloud-resolving model (Soong and Ogura, 1980; Soong and Tao, 1980; Tao and Simpson, 1993) used in this study is the 2D version of a model (Sui et al., 1994, 1998) modified by Li et al. (1999). The model with cyclic lateral boundaries includes five prognostic equations for the mixing ratios of cloud water, raindrops, cloud ice, snow, and graupel. The model uses the cloud microphysical parameterization schemes taken from Rutledge and Hobbs (1983, 1984), Lin et al. (1983), Tao et al. (1989), and Krueger et al. (1995) and solar (Chou et al., 1998) and thermal infrared (Chou et al., 1991; Chou and Suarez, 1994) radiation parameterization schemes are performed every 3 minutes. The model parameters include a horizontal domain of 768 km, a horizontal grid resolution of 1.5 km, 33 vertical levels, and a time step of 12 s. The model is forced by the imposed zonally-uniform vertical velocity, zonal wind, and horizontal temperature and vapor advection. The detailed model descriptions can be found in Gao and Li (2008).

The budgets of mass-integrated water vapor mixing ratio and cloud hydrometeor mixing ratio can be, respectively, written as

$$Q_{\rm WVT}+Q_{\rm WVF}+Q_{\rm WVE}=Q_{\rm WVOUT}+Q_{\rm WVIN}\ , \quad (1)$$

and

$$P_{\rm s}-Q_{\rm CM}=Q_{\rm WVOUT}+Q_{\rm WVIN}, \quad (2)$$

where

$$Q_{\rm WVT}=-\frac{[\partial q_{\rm v}]}{\partial t}\ , \quad (3a)$$

$$Q_{\rm WVF}=-\left[\overline{u}_{\rm o}\frac{\partial \overline{q}_{\rm v,o}}{\partial x}\right]-\left[\overline{w}_{\rm o}\frac{\partial \overline{q}_{\rm v}}{\partial z}\right]-\left[\frac{\partial(u'q'_{\rm v})}{\partial x}\right]-\left[\overline{u}_{\rm o}\frac{\partial q'_{\rm v}}{\partial x}\right]-\left[\overline{w}_{\rm o}\frac{\partial q'_{\rm v}}{\partial z}\right]-\left[w'\frac{\partial \overline{q}_{\rm v}}{\partial z}\right]\ , \quad (3b)$$

$$Q_{\rm WVE}=E_{\rm s}\ , \quad (3c)$$

$$Q_{\rm CM}=-\frac{\partial[q_5]}{\partial t}-\left[\frac{\partial(uq_5)}{\partial x}\right]\ . \quad (3d)$$

Here, $q_{\rm v}$ is specific humidity; u and w are zonal and vertical wind components, respectively; $E_{\rm s}$ is surface

evaporation rate; $q_5 = q_c + q_r + q_i + q_s + q_g$, and q_c, q_r, q_i, q_s, q_g are the mixing ratios of cloud water, raindrops, cloud ice, snow, and graupel, respectively; $Q_{WVOUT}(=[P_{CND}]+[P_{DEP}]+[P_{SDEP}]+[P_{GDEP}])$ represents the sink term in the water vapor budget and the source term in the cloud budget that consists of the vapor condensation rate ($[P_{CND}]$), vapor deposition rates for the growth of cloud ice ($[P_{DEP}]$), snow ($[P_{SDEP}]$), and graupel ($[P_{GDEP}]$); $Q_{WVIN}(=-[P_{REVP}]-[P_{MLTG}]-[P_{MLTS}])$ denotes the source term in the water vapor budget and the sink term in the cloud budget that include growth of vapor by evaporation of raindrops ($[P_{REVP}]$), melting graupel ($[P_{MLTG}]$), and melting snow ($[P_{MLTS}]$); overbars denotes a domain-mean; primed quantities are perturbations from the domain mean; $[(\ )] = \int_{z_b}^{z_t} \overline{\rho}(\ )dz$, and z_t and z_b are the heights of the top and bottom of the model atmosphere respectively; and the subscript o denotes an imposed GDAS-observed value. The local water vapor change is determined by water vapor convergence, surface evaporation, and cloud microphysical processes, including vapor condensation and deposition and evaporation of rain in the water vapor budget (1). The local hydrometeor change is determined by hydrometeor convergence, surface rain rate, and cloud microphysical processes in the cloud budget (2).

Following Gao et al. (2005a) and Cui and Li (2006), the surface rainfall equation is derived by subtracting (1) from (2),

$$P_s = Q_{WVT} + Q_{WVF} + Q_{WVE} + Q_{CM}. \quad (4)$$

The surface rainfall budget (4) states that surface rain rate is contributed to by the local vapor change (Q_{WVT}), vapor convergence (Q_{WVF}), surface evaporation (Q_{WVE}), and cloud source/sink (Q_{CM}). Positive Q_{WVT}, Q_{WVF}, and Q_{CM} denote local vapor loss (atmospheric drying), vapor convergence, and local hydrometeor loss/hydrometeor convergence, respectively, whereas negative Q_{WVT}, Q_{WVF}, and Q_{CM} denote local vapor gain (atmospheric moistening), vapor divergence, and local hydrometeor gain/hydrometeor divergence, respectively.

The thermal budget can be expressed as

$$S_{HT} + S_{HF} + S_{HS} + S_{LH} + S_{RAD} = 0\ , \quad (5)$$

where

$$S_{HT} = -\frac{\partial < T >}{\partial t}\ , \quad (5a)$$

$$S_{HF} = - < \overline{u}_o \frac{\partial \overline{T}_o}{\partial x} > - < \pi \overline{w}_o \frac{\partial \overline{\theta}}{\partial z} > - < \frac{\partial (u'T')}{\partial x} > - < \overline{u}_o \frac{\partial T'}{\partial x} > - < \pi \overline{w}_o \frac{\partial \theta'}{\partial z} > - < \pi \frac{\partial \overline{\theta}}{\partial z} >\ , \quad (5b)$$

$$S_{HS} = H_s\ , \quad (5c)$$

$$S_{LH} = \frac{1}{c_p} < Q_{cn} >\ , \quad (5d)$$

$$S_{RAD} = \frac{1}{c_p} < Q_R >\ . \quad (5e)$$

Here, T and θ are air temperature and potential temperature, respectively, c_p is the specific heat of dry air at constant pressure, and H_s is the surface sensible heat flux. Q_{cn} can be expressed as

$$Q_{cn} = L_v(P_{CND} - P_{REVP}) + L_s(P_{DEP} + P_{SDEP} + P_{GDEP} - P_{MLTG}) + L_f\{P_{SACW} + P_{GACW}(T < T_o) - P_{RACS} - P_{SMLT} - P_{GMLT}\ , \quad (6)$$

where L_v, L_s, and L_f are the latent heats of vaporization, sublimation, and fusion at 0°C, respectively, with $L_s = L_v + L_f$. P_{SACW} and P_{GACW} are the accretion of cloud water by snow and graupel, respectively; P_{RACS} is the accretion of snow by raindrops; P_{SMLT} and P_{GMLT} represent melting of snow and graupel into raindrops, respectively; Q_R is the radiative heating rate due to the convergence of the net flux of solar and infrared radiative fluxes, and

$$< (\ ) > = \int_{z_b}^{z_t} \overline{\rho}(\ )dz \Big/ \int_{z_b}^{z_t} \overline{\rho} dz\ .$$

The thermal budget (6) states that local heat change (S_{HT}) is determined by thermal convergence (S_{HF}), surface sensible heat flux (S_{HS}), condensational heating (S_{LH}), and radiative heating (S_{RAD}).

Surface rainfall is partitioned into convective and stratiform rainfall. Convective and stratiform rainfall are caused by different cloud microphysical processes and vertical profiles of vertical velocity (e.g., Houghton, 1968; Li et al., 2002) and their associated clouds have different radiative effects on atmospheric thermodynamics (e.g., Gao et al., 2006; Ping et al., 2007; Gao et al., 2007). Thus, convective and stratiform rainfall processes are analyzed in this study. Convective-stratiform rainfall partitioning has been based mainly on the amplitude and spatial variations of radar reflectivity or surface rainfall rate (e.g., Churchill and Houze, 1984; Caniaux et al., 1994; Steiner et al., 1995) and modified by additional information like cloud contents, vertical motion, and the fall speed of precipitation particles (e.g., Tao and Simpson, 1989; Tao et al., 1993, 2000; Sui et al., 1994; Xu, 1995; Lang et al., 2003). The partition method originally developed by Tao and Simpson (1993) and modified by Sui et al. (1994) is used in this study. In

this method, a model grid point is identified as convective if a rain rate at this grid point is twice as large as the average taken over the surrounding four grid points (two grid points on either side of this grid point in the two-dimensional framework), or a rain rate at this grid point is greater than 20 mm h^{-1}. All non-convective cloudy grid points are considered as stratiform. Additional information based on cloud hydrometeors and vertical velocity is used to further detect convective grid points in stratiform regions.

The 2D and three-dimensional (3D) models produce similar simulations of collective thermodynamic feedback effects, vertical transports of mass, sensible heat, and moisture, thermodynamic fields, surface heat fluxes, surface precipitation, precipitation efficiency, and convective and moist vorticity vectors (e.g., Tao and Soong, 1986; Tao et al., 1987; Grabowski et al., 1998; Tompkins, 2000; Khairoutdinov and Randall, 2003; Gao et al., 2004, 2005b, 2007; Sui et al., 2005). Xu et al. (2002) carried out an intercomparison study of cloud-resolving models during the Atmospheric Radiation Measurement (ARM) project and found that some differences between 2D and 3D model simulations may be caused by the small model domain size in the 3D model and the differences between 2D and 3D dynamics. Gao et al. (2005b) and Gao (2008) revealed that the horizontal component of the dynamic vorticity vector has a close relation with convection in the 3D model framework, whereas the vertical component has an intimate relation with convection in the 2D model framework. This is due to the exclusion of dominant items in the horizontal components of the 3D dynamic vorticity vector from the 2D model framework. It should be noted that the difference in dynamics between the 2D and 3D is due to the difference between the 3D and 2D frameworks instead of due to the difference in the 2D and 3D wind fields. In fact, the model domain mean wind in this study is imposed by NCEP/GDAS data at each time step. Since this study focuses on a budgetary analysis of water vapor, heat, cloud, and surface rainfall, the 2D model can be used to conduct this study.

3. Results

Typhoon Krosa (2007) formed in the Pacific east of the Philippines at 0800 LST 2 October 2007. It strengthened to a super typhoon around the early morning of 5 October. Krosa made landfall twice over Yilan County of Taiwan at 1530 LST and 2230 LST 6 October. It did counterclockwise looping for nearly 7 hours between landfalls. Later, Krosa crossed northeast Taiwan to enter the northern Taiwan Straits while it was weakening. Krosa made another landfall over the coast at the intersection between Zhejiang Province and Fujian Province at 1530 LST 7 October. The maximum wind was 33 m s^{-1} during the landfall. Krosa brought torrential rainfall over the eastern coast of China including Shanghai from 7–8 October. Figure 1 summarizes the large-scale circulation surrounding Krosa during the landfall using wind and geopotential height data at 700 hPa from the National Centers for Environmental Prediction (NCEP)/Global Data Assimilation System (GDAS). On 6 October 2007, Krosa was approaching the eastern coast of China with strong cyclonic winds in the lower troposphere, surrounded by an intensifying trough to its northeast and weak highs to its west. One day later, it continued its landfalling course while a trough to its north strengthened rapidly to form a low. On 8 October, a weak high formed to block the inland movement of Krosa while it was pouring down rain over the eastern coast. Note that the trough developed into an extratropical cyclone to the north of Krosa from 6 to 7 October, and the intensification and southward movement of the extratropical cyclone caused frontal genesis associated with Krosa during its landfall.

The meridionally oriented rectangular area of 28°–32°N, 121°–122°E was chosen for averaging the forcing data that are imposed in the model because the maximum rainfall occurred over this area and the rainbands showed a meridional orientation (not shown). The zonally-uniform vertical velocity, zonal wind, and horizontal temperature and vapor advection that are imposed in the model (Fig. 2) are calculated using NCEP/GDAS data with a horizontal resolution of $1° \times 1°$ and a temporal resolution of 4 times per day. The data include geopotential height, temperature, relative humidity, zonal and meridional wind, and vertical velocity. The model is integrated from 0800 LST 6 October to 0800 LST 9 October 2007 (a total of 3 days) during the landfall. Figure 3 shows similarity in surface rain rates between the simulation and rain gauge observations. The root-mean-squared (RMS) difference in surface rain rates between the simulation and rain gauge observations is 1.04 mm h^{-1}, which is smaller than the standard derivations of the simulated rain rate (1.16 mm h^{-1}) and the observed rain rate (1.18 mm h^{-1}). The large difference in the late evening of 6 October, the evening of 7 October, and the late afternoon of 8 October (Fig. 3) mainly contribute to the large RMS difference in rain rate between the simulation and observations. The total hydrometeor mixing ratio (sum of mixing ratios of cloud water, raindrops, cloud ice, snow, and graupel) cannot extend to the upper troposphere in the morning and afternoon of 6 October (Fig. 4) due to the weak downward motion imposed in the model (Fig. 2a). The imposed upward

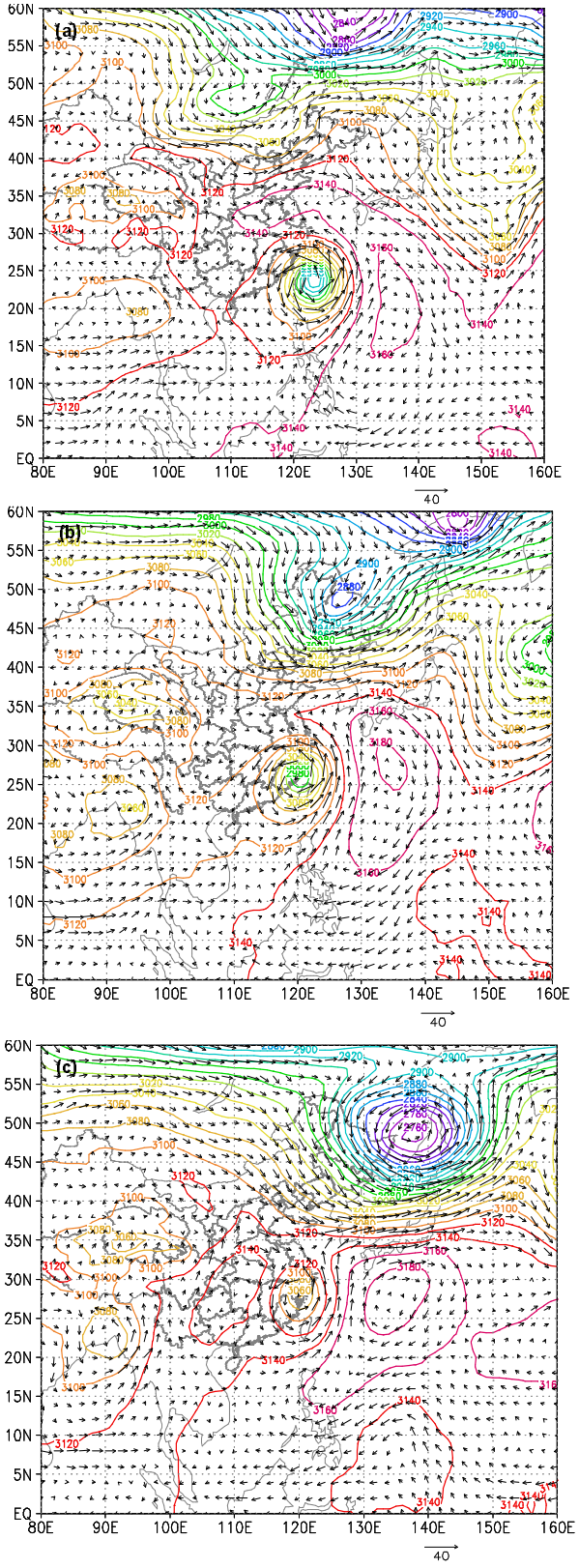

Fig. 1. Geopotential height (m) and wind ($m\,s^{-1}$) fields at 700 hPa for (a) 0800 LST 6 October, (b) 0800 LST 7 October, and (c) 0800 LST 8 October 2008.

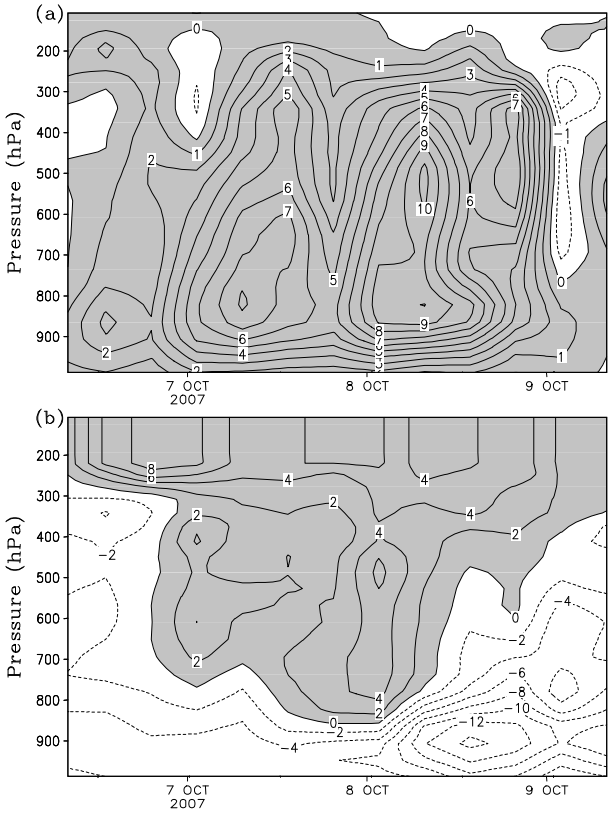

Fig. 2. Temporal and vertical distribution of (a) vertical velocity (cm s^{-1}) and (b) meridional wind (m s^{-1}) averaged over 28°–32°N, 121°–122°E from NCEP/GDAS data. Upward motion in (a) and southerly wind in (b) are shaded.

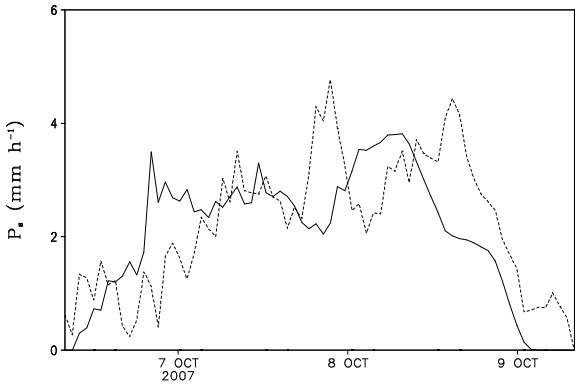

Fig. 3. Time series of simulated (dashed) and observed (solid) surface rain rates (mm h^{-1}).

motion intensifies and extends to the upper troposphere, which causes a large total hydrometeor mixing ratio in the upper troposphere and large surface rainfall (Fig. 3) in the late evening of 6 October. The peaks of imposed upward motions lead to the maximum total

Table 1. Time means of the fractional cloud coverage and water vapor budget (1) over raining stratiform and convective regions and their sums (model domain means) averaged (a) from 1200 LST to 2300 LST 6 October, (b) on 7 October, and (c) on 8 October 2007. Units are % for fractional cloud coverage and mm h^{-1} for the others.

		Raining stratiform regions	Convective regions	Model domain mean
(a)	Fractional coverage	77.7	21.1	100.0
	Q_{WVT}	−0.890	−0.245	−1.147
	Q_{WVF}	1.997	1.119	3.129
	Q_{WVE}	0.019	0.006	0.025
	Q_{WVOUT}	1.287	0.902	2.191
	Q_{WVIN}	−0.161	−0.023	−0.184
(b)	Fractional coverage	84.8	15.2	100.0
	Q_{WVT}	0.378	−0.015	0.363
	Q_{WVF}	1.757	0.493	2.250
	Q_{WVE}	0.022	0.002	0.023
	Q_{WVOUT}	2.208	0.485	2.693
	Q_{WVIN}	−0.051	−0.005	−0.056
(c)	Fractional coverage	97.7	2.3	100.0
	Q_{WVT}	1.195	0.035	1.230
	Q_{WVF}	0.893	0.055	0.947
	Q_{WVE}	0.299	0.006	0.305
	Q_{WVOUT}	2.624	0.101	2.725
	Q_{WVIN}	−0.238	−0.004	−0.242

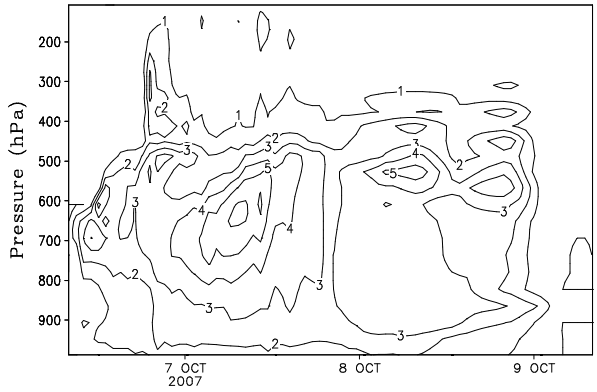

Fig. 4. Temporal and vertical distribution of simulated model domain mean total hydrometeor mixing ratio (10^{-1} g kg^{-1}).

hydrometeor mixing ratios (0.5–0.6 g kg^{-1}) in the late mornings of 7 and 8 October, respectively.

3.1 *Water vapor and heat budgets*

The water vapor budget links water vapor and cloud hydrometeors [see Eq. (1)]. Water vapor budgets including net condensation as the important role in convective development have been examined in previous studies (e.g., Tao and Simpson, 1993; Johnson et al., 2007). Figure 2a shows that upward motion gradually extended to the troposphere on 6 October, and upward motion reached its maximum of 7 cm s^{-1} in the lower troposphere one day later, with a peak of 10 cm s^{-1} in the mid troposphere on 8 October. To examine rainfall and cloud responses to the large-scale forcing, the temporally averaged budgets are analyzed on 6, 7, and 8 October, respectively. Note that the simulation data from 1200 LST to 2300 LST 6 October 2007 are analyzed in this study. The budgets were also calculated using the simulation data from 0800 LST to 2300 LST 6 October, and the results are similar to those discussed in this study. Time and model domain mean water vapor budgets (Table 1) show that the vapor convergence rates (Q_{WVF}) decreased from 3.129 mm h^{-1} on 6 October to 0.947 mm h^{-1} on 8 October 2007 while vapor condensation and deposition rates (Q_{WVOUT}) increased from 2.191 mm h^{-1} on 6 October to 2.725 mm h^{-1} on 8 October 2007 and Q_{WVT} switched from a negative value on 6 October to positive values on 7 and 8 October 2007. The vapor convergence supported both vapor condensation/deposition and local atmospheric moistening on 6 October. Vapor condensation/deposition consumed water vapor from vapor convergence and led to local atmospheric drying on 7 and 8 October.

Heat budgets associated with convective development have been analyzed (e.g., Tao and Simpson, 1993; Xu, 1995; Tao et al., 2004). Here, time and model domain mean heat budgets reveal that S_{HF}, S_{LH}, and S_{HT} are much larger than S_{RAD} and S_{HS} (Table 2). On 6 October 2007, the latent heating rate is larger than the advective cooling rate, causing a local atmospheric warming. On 7 October, the latent heating rate becomes slightly smaller than the advective cooling rate, which leads to a weak local atmospheric cooling. One day later, the advective cooling intensifies while the latent heating rate is nearly constant. As a result, the

Table 2. Time and model domain means of the heat budget (5) averaged from 1200 LST to 2300 LST on 6 October, 7 October, and 8 October 2007, respectively. Units: $^{\circ}$C h^{-1}.

	6 October	7 October	8 October
S_{RAD}	−0.005	−0.020	−0.005
S_{HT}	−0.185	0.097	0.231
S_{HF}	−0.275	−0.760	−0.926
S_{HS}	0.007	0.009	0.040
S_{LH}	0.457	0.675	0.661

local atmosphere continues its cooling course.

The water vapor budgets are further calculated for convective and stratifrom rainfall (Table 1). Nonraining stratiform clouds cover a very small area (1.2%) on 6 October 2007 and their associated water vapor budget is excluded from Table 1. Fractional coverage of convective rainfall decreases, while that of stratiform rainfall increases steadily over the three days. On 6 October 2007, the water vapor convergence rates are larger than vapor condensation and deposition rates over both raining stratiform and convective regions, which results in local atmospheric moistening. One day later, the water vapor convergence rate becomes smaller than the vapor condensation and deposition rates over the raining stratiform regions, while it remains larger over the convective regions. Thus, local atmospheric drying occurs over the raining stratiform regions, which contributes to the time and model domain mean local atmospheric drying. On 8 October, the vapor convergence rate becomes smaller than the vapor condensation and deposition rates over the convective regions. Local atmospheric drying appears over both the raining stratiform and convective regions. From the above discussion, surface rainfall is not an explicit item in the water vapor budget [see Eq. (1)]. However, surface rainfall has a direct linkage to cloud development in the cloud budget. Therefore, the cloud budget will be discussed next.

3.2 *Cloud budget*

Surface rain rate is a part of the cloud budget [see Eq. (2)], which links surface rainfall and clouds. The analysis of cloud budgets has been conducted to study convective systems in the tropics and midlatitudes (e.g., Gamache and Houze, 1983; Rutledge and Houze, 1987; Chong and Hauser, 1989; Gallus and Johnson, 1991). The time and model domain mean surface rain rate increased from 1.794 mm h^{-1} on 6 October to 2.586 mm h^{-1} on 7 October and kept a similar value for another day (Table 3). During the three days, Q_{WVOUT} was at least one order of magnitude larger than Q_{WVIN} and Q_{CM}. Thus, the vapor condensation and deposition rates largely determined the mean surface rain rate. Analyzing the cloud microphysics precipitation efficiency (CMPE) (e.g., Sui et al., 2007) provides a way to measure how well surface rain rate is estimated by the vapor condensation and deposition rates. CMPE can be written as

$$\mathrm{CMPE} = \frac{P_{\mathrm{s}}}{Q_{\mathrm{WVOUT}}} \,. \tag{7}$$

CMPE calculated from time and model domain mean data could be in the range 82%–96%, which suggests that Q_{WVOUT} cannot accurately represent surface rain rate.

Table 3. Time means of the cloud budget (2) and CMPE (7) over raining stratiform and convective regions and their sums (model domain means) averaged from 1200 LST to 2300 LST on (a) 6 October, (b) 7 October, and (c) 8 October 2007. Units are % for CMPE and mm h^{-1} for the others.

		Raining stratiform regions	Convective regions	Model domain mean
(a)	P_{s}	1.311	0.483	1.794
	Q_{CM}	0.185	−0.396	−0.213
	Q_{WVOUT}	1.287	0.902	2.191
	Q_{WVIN}	−0.161	−0.023	−0.184
	CMPE	101.9	53.5	81.9
(b)	P_{s}	2.311	0.275	2.586
	Q_{CM}	0.154	−0.204	−0.050
	Q_{WVOUT}	2.208	0.485	2.693
	Q_{WVIN}	−0.051	−0.005	−0.056
	CMPE	104.7	56.7	96.0
(c)	P_{s}	2.480	0.084	2.564
	Q_{CM}	0.094	−0.013	0.081
	Q_{WVOUT}	2.624	0.101	2.725
	Q_{WVIN}	−0.238	−0.004	−0.242
	CMPE	94.5	83.2	94.1

On 6 October 2007, 73.1% and 26.9% of the time and model domain mean surface rain rate come from raining stratiform and convective regions, respectively. Values of 89.4% and 96.7% for the time and model domain mean surface rain rate contribution by stratiform rain rate are simulated on 7 and 8 October, respectively. $Q_{\rm WVOUT}$ nearly accounts for the stratiform rain rate during the three days, as indicated by the values of CMPE (∼100%). Convective rain rate only consumes about 50%–85% of $Q_{\rm WVOUT}$. Large differences between $Q_{\rm WVOUT}$ and $P_{\rm s}$ over convective regions are due to large $Q_{\rm CM}$, which represents transport of cloud hydrometeors from convective regions to raining stratiform regions, as well as the increase of cloud hydrometeors over convective regions. The increase of time mean cloud hydrometeors over convective regions is responsible for the increase of time and model domain mean cloud hydrometeors.

3.3 *Surface rainfall budget*

Since surface rain rate is not included in the water vapor budget and it could be significantly different from vapor condensation and deposition rates, surface rainfall processes cannot be properly addressed in either the water vapor or cloud budgets. For example, large-scale precipitation efficiency (LSPE) cannot be properly defined as indicated by Li et al. (2002) and Sui et al. (2005), in which LSPE1 is defined by

$$\text{LSPE1} = \frac{P_{\rm s}}{Q_{\rm WVF} + Q_{\rm WVE}} \,. \tag{8}$$

LSPE1 cannot be defined from the water vapor budget because surface rain rate is not a component in the water vapor budget or the cloud budget because vapor convergence and surface evaporation are not included in the cloud budget. As a result, LSPE1 could be negative or larger than 100%, which is not physically meaningful. Gao et al. (2005a) combined the water vapor budget and cloud budget into the surface rainfall budget (4). In the surface rainfall budget, the contributions of water vapor processes and cloud processes to surface rainfall can be analyzed in the same framework. Wang et al. (2007) analyzed surface rainfall processes during the South China Sea Monsoon Experiment (SCSMEX) and found that $Q_{\rm WVT}$ and $Q_{\rm CM}$ could be positive. These indicate the local atmospheric drying and the decrease of local cloud hydrometeors contribute to surface rainfall but they are not included in Eq. (8) as sources of surface rainfall, which leads to LSPE1 values of larger than 100%. Sui et al. (2007) analyzed LSPE using Eq. (8) and found that negative LSPE1 occurs over subsidence regions where vapor divergence rate is larger than the surface evaporation rate. Sui et al. (2007) introduced a new definition for LSPE, which can be expressed as

$$\text{LSPE2} = \frac{P_{\rm s}}{\sum_{i=1}^{4} H(Q_i) Q_i} \,, \tag{9}$$

where $Q_i = (Q_{\rm WVT}, Q_{\rm WVF}, Q_{\rm WVE}, Q_{\rm CM})$; H is the Heaviside function, $H(F) = 1$ when $F > 0$, and $H(F) = 0$ when $F \leqslant 0$. The surface rainfall budget has been used to study convective development and surface rainfall processes in the tropics and midlatitudes (e.g., Gao et al., 2005a, 2006; Cui and Li, 2006; Ping et al., 2007; Wang et al., 2007; Xu et al., 2007).

The time and model domain mean surface rainfall budget shows that on 6 October 2007, 56.9% of the water vapor source ($Q_{\rm WVF} + Q_{\rm WVE}$) supports surface rainfall as indicated by LSPE2 (Table 4). It is found that 36.4% and 6.8% of the water vapor source goes to local atmospheric moistening and the increase of cloud hydrometeor concentrations, respectively. One day later, in addition to the vapor convergence and surface evaporation, the local atmospheric drying (positive $Q_{\rm WVT}$) becomes a water vapor source. Thus, LSPE2 increases to 98.1%. On 8 October, the decrease of cloud hydrometeor concentration (negative $Q_{\rm CM}$) is also a water vapor source, so that LSPE2 is 100.0%. It is interesting to note that the vapor convergence rate decreases with time while the surface rain rate increases. The local atmosphere switches from a moistening trend on 6 October to drying on 7 October, and the local atmospheric drying rate increases on 8 October. The cloud hydrometeor concentration increases during 6–7 October and starts to decrease on 8 October.

Over raining stratiform regions, LSPE2 is 59.6% due to the local atmospheric moistening on 6 October 2007. LSPE2 becomes 100% one day later after the local atmosphere switches to drying. Over convective regions, LSPE2 increases with time while the vapor convergence rate, the local atmospheric moistening rate, and the growth rate of cloud hydrometeor concentration decrease.

4. Summary

Water vapor, cloud, surface rainfall, and heat budgets associated with the landfall of Typhoon Krosa over the eastern coast of China in October 2007 are examined using a two-dimensional cloud-resolving model simulation. The model is integrated for 3 days with imposed zonally-uniform vertical velocity, zonal wind, horizontal temperature and vapor advection from NCEP/GDAS data. Simulated model domain mean surface rain rates are generally in agreement with rain gauge data. Thus, the simulation data are further used to study the surface rainfall processes.

Table 4. Time means of the surface rainfall budget (4) and LSPE2 (9) over raining stratiform and convective regions and their sums (model domain means) averaged from 1200 LST to 2300 LST on (a) 6 October, (b) 7 October, and (c) 8 October 2007. Units are % for fractional cloud coverage and LSPE2 and mm h^{-1} for the others.

		Raining stratiform regions	Convective regions	Model domain mean
(a)	P_s	1.311	0.483	1.794
	Q_{WVT}	−0.890	−0.245	−1.147
	Q_{WVF}	1.997	1.119	3.129
	Q_{WVE}	0.019	0.006	0.025
	Q_{CM}	0.185	−0.396	−0.213
	LSPE2	59.6	42.9	56.9
(b)	P_s	2.311	0.275	2.586
	Q_{WVT}	0.378	−0.015	0.363
	Q_{WVF}	1.757	0.493	2.250
	Q_{WVE}	0.022	0.002	0.023
	Q_{CM}	0.154	−0.204	−0.050
	LSPE2	100.0	55.6	98.1
(c)	P_s	2.480	0.084	2.564
	Q_{WVT}	1.195	0.035	1.230
	Q_{WVF}	0.893	0.055	0.947
	Q_{WVE}	0.299	0.006	0.305
	Q_{CM}	0.094	−0.013	0.081
	LSPE2	100.0	87.5	100.0

The time and model domain mean budgets are first examined. On 6 October 2007, Typhoon Krosa approached the eastern coast of China, and ascending motion appeared over the eastern coastal area. The water vapor from the open ocean surface along with the ascending motion induced large water vapor convergence. The vapor convergence led to local atmospheric moistening, surface rainfall, and cloud development through vapor condensation and deposition. Meanwhile, latent heating overcame advective cooling to yield a local atmospheric warming. As the typhoon made landfall on 7 October, a large part of the storm covered the land area and the water vapor source was cut off, thus weakening vapor convergence. The increase of vapor condensation and deposition rates associated with the increase of the surface rain rate caused local atmospheric drying. At the same time, both advective cooling and latent heating rates increased, but the former increased faster than the latter did, leading to a weak local atmospheric cooling. On 8 October, less water vapor was available for continuous convective development, as indicated by the small vapor convergence rate. Thus, the large vapor condensation and deposition maintained the surface rain rate while significantly drawing down local water vapor. The advective cooling rate increased while the latent heating rate stopped its increase, which increased the local atmospheric cooling rate.

Fractional coverage of raining stratiform clouds increases as convective rainfall decreases. Since the model domain is dominated by raining stratiform, the water vapor, cloud, and surface rainfall budgets over raining stratiform regions are similar to those in the model domain mean. Over convective regions, the convective rain rate, local atmospheric moistening rate, and growth rate of cloud hydrometeor concentration decrease with decreasing vapor convergence rate.

Acknowledgements. Authors thank Dr. W.-K. Tao at NASA/GSFC for his cloud-resolving model and two anonymous reviewers for their constructive comments. This research is supported by the National Natural Science Foundation of China (Grants Nos. 40875025, 40875030, and 40775033), and the Shanghai Natural Science Foundation of China (Grant No. 08ZR1422900).

REFERENCES

Bender, M., A., R. E. Tuleya, and Y. Kurihara, 1985: A numerical study of the effect of a mountain range on a landfalling tropical cyclone. *Mon. Wea. Rev.*, **113**, 567–582.

Caniaux, G., J.-L. Redelsperger, and J.-P. Lafore, 1994: A numerical study of the stratiform region of a fast-moving squall line. Part I: General description and water and heat budgets. *J. Atmos. Sci.*, **51**, 2046–2074.

Chen, L., Z. Luo, and Y. Li, 2004: Research advances on tropical cyclone landfall process. *Acta Meteorologica Sinica*, **62**, 541–549. (in Chinese)

Chong, M., and D. Hauser, 1989: A tropical squall line observed during the COPT 81 experiment in West Africa. Part II: Water budget. *Mon. Wea. Rev.*, **117**, 728–744.

Chou, M.-D., and M. J. Suarez, 1994: An efficient thermal infrared radiation parameterization for use in gen-

eral circulation model. NASA Tech. Memo. 104606, Vol. 3, 85pp. [Available from NASA/Goddard Space Flight Center, Code 913, Greenbelt, MD 20771.]

Chou, M.-D., D. P. Kratz, and W. Ridgway, 1991: Infrared radiation parameterization in numerical climate models. *J. Climate*, **4**, 424–437.

Chou, M.-D., M. J. Suarez, C.-H. Ho, M. M.-H. Yan, and K.-T. Lee, 1998: Parameterizations for cloud overlapping and shortwave single scattering properties for use in general circulation and cloud ensemble models. *J. Atmos. Sci.*, **55**, 201–214.

Churchill, D. D., and R. A. Houze, Jr., 1984: Development and structure of winter monsoon cloud clusters on 10 December 1978. *J. Atmos. Sci.*, **41**, 933–960.

Colle, B. A., 2003: Numerical simulations of the extratropical transition of Floyd (1999): Structural evolution and responsible mechanisms for the heavy rainfall over the Northeast United States. *Mon. Wea. Rev.*, **131**, 2905–2926.

Cui, X., and X. Li, 2006: Role of surface evaporation in surface rainfall processes. *J. Geophys. Res.*, **111**, D17112, doi: 10.1029/2005JD006876.

Elsberry, R. L., 2002: Predicting hurricane landfall precipitation: Optimistic and pessimistic views from the symposium on precipitation extremes. *Bull. Amer. Meteor. Soc.*, **83**, 1333–1339.

Elsberry, R. L., and F. D. Marks, 1999: The hurricane landfall workshop summary. *Bull. Amer. Meteor. Soc.*, **80**, 683–685.

Gallus, W. A., Jr., and R. H. Johnson, 1991: Heat and moisture budgets of an intense midlatitude squall line. *J. Atmos. Sci.*, **48**, 122–146.

Gamache, J. F., and R. A. Houze, Jr., 1983: Water budget of a mesoscale convective system in the tropics. *J. Atmos. Sci.*, **40**, 1835–1850.

Gao, S., 2007: A cloud-resolving modeling study of cloud radiative effects on tropical equilibrium states. *J. Geophys. Res.*, **112**, doi: 10.1029/2007JD009177.

Gao, S., 2008: A three dimensional dynamic vorticity vector associated with tropical oceanic convection. *J. Geophys. Res.*, **113**, doi: 10.1029/2006JD008247.

Gao, S., and X. Li, 2008: *Cloud-Resolving Modeling of Convective Processes*. Springer, Dordrecht, 206pp.

Gao, S., F. Ping, X. Li, and W.-K. Tao, 2004: A convective vorticity vector associated with tropical convection: A two-dimensional cloud-resolving modeling study. *J. Geophys. Res.*, **109**, D14106, doi: 10.1029/2004JD004807.

Gao, S., X. Cui, Y. Zhu, and X. Li, 2005a: Surface rainfall processes as simulated in a cloud resolving model. *J. Geophys. Res.*, **110**, D10202, doi: 10.1029/2004JD005467.

Gao, S., X. Cui, Y. Zhou, X. Li, and W.-K. Tao, 2005b: A modeling study of moist and dynamic vorticity vectors associated with 2D tropical convection. *J. Geophys. Res.*, **110**, D17104, doi: 10.1029/2004JD005675.

Gao, S., L. Ran, and X. Li, 2006: Impacts of ice microphysics on rainfall and thermodynamic processes in the tropical deep convective regime: A 2D cloud-resolving modeling study. *Mon. Wea. Rev.*, **134**, 3015–3024.

Gao, S., X. Li, W.-K. Tao, C.-L. Shie, and S. Lang, 2007: Convective and moist vorticity vectors associated with tropical oceanic convection: A three-dimensional cloud-resolving simulation. *J. Geophys. Res.*, **112**, D01105, doi: 10.1029/2006JD7179.

Grabowski, W. W., X. Wu, and M. W. Moncrieff, 1996: Cloud-resolving model of tropical cloud systems during Phase III of GATE. Part I: Two-dimensional experiments. *J. Atmos. Sci.*, **53**, 3684–3709.

Grabowski, W. W., X. Wu, M. W. Moncrieff, and W. D. Hall, 1998: Cloud-resolving model of tropical cloud systems during Phase III of GATE. Part II: Effects of resolution and the third spatial dimension. *J. Atmos. Sci.*, **55**, 3264–3282.

Houghton, H. G., 1968: On precipitation mechanisms and their artificial modification. *J. Appl. Meteor.*, **7**, 851–859.

Ji, C., G. Xue, F. Zhao, Z. Yu, and H. Zhang, 2007: The numerical simulation of orographic effect on the rain and structure of typhoon Rananim during landfall. *Chinese J. Atmos. Sci.*, **31**, 233–244 (in Chinese).

Johnson, D., W.-K. Tao, and J. Simpson, 2007: A study of the response of deep tropical clouds to mesocale processes, Part II: Sensitivity tests of radiation, surface fluxes and microphysics. *J. Atmos. Sci.*, **64**, 869–886.

Khairoutdinov, M. F., and D. A. Randall, 2003: Cloud-resolving modeling of the ARM summer 1997 IOP: Model formulation, results, uncertainties, and sensitivities. *J. Atmos. Sci.*, **60**, 607–625.

Krueger, S. K., Q. Fu, K. N. Liou, and H.-N. S. Chin, 1995: Improvement of an ice-phase microphysics parameterization for use in numerical simulations of tropical convection. *J. Appl. Meteor.*, **34**, 281–287.

Lang, S., W.-K. Tao, J. Simpson, and B. Ferrier, 2003: Modeling of convective-stratiform precipitation processes: Sensitivity to partition methods. *J. Appl. Meteor.*, **42**, 505–527.

Li, X., C.-H. Sui, K.-M. Lau, and M.-D. Chou, 1999: Large-scale forcing and cloud-radiation interaction in the tropical deep convective regime. *J. Atmos. Sci.*, **56**, 3028–3042.

Li, X., C.-H. Sui, and K.-M. Lau, 2002: Dominant cloud microphysical processes in a tropical oceanic convective system: A 2-D cloud resolving modeling study. *Mon. Wea. Rev.*, **130**, 2481–2491.

Lin, Y.-L., R. D. Farley, and H. D. Orville, 1983: Bulk parameterization of the snow field in a cloud model. *J. Climate Appl. Meteor.*, **22**, 1065–1092.

Ping, F., Z. Luo, and X. Li, 2007: Microphysical and radiative effects of ice microphysics on tropical equilibrium states: A two-dimensional cloud-resolving modeling study. *Mon. Wea. Rev.*, **135**, 2794–2802.

Rutledge, S. A., and P. V. Hobbs, 1983: The mesoscale and microscale structure and organization of clouds and precipitation in midlatitude cyclones. Part VIII:

A model for the "seeder-feeder" process in warm-frontal rainbands. *J. Atmos. Sci.*, **40**, 1185–1206.

Rutledge, S. A., and P. V. Hobbs, 1984: The mesoscale and microscale structure and organization of clouds and precipitation in midlatitude cyclones. Part XII: A diagnostic modeling study of precipitation development in narrow cold-frontal rainbands. *J. Atmos. Sci.*, **41**, 2949–2972.

Rutledge, S. A., and R. A. Houze, Jr., 1987: A diagnostic modeling study of the trailing stratiform rain of a mid latitude squall line. *J. Atmos. Sci.*, **44**, 2640–2656.

Soong, S. T., and Y. Ogura, 1980: Response of tradewind cumuli to large-scale processes. *J. Atmos. Sci.*, **37**, 2035–2050.

Soong, S. T., and W.-K. Tao, 1980: Response of deep tropical cumulus clouds to Mesoscale processes. *J. Atmos. Sci.*, **37**, 2016–2034.

Steiner, M., R. A. Houze Jr., and S. E. Yuter, 1995: Climatological characterization of three-dimensional storm structure from operational radar and rain gauge data. *J. Appl. Meteor.*, **34**, 1978–2007.

Sui, C.-H., K.-M. Lau, W.-K. Tao, and J. Simpson, 1994: The tropical water and energy cycles in a cumulus ensemble model. Part I: Equilibrium climate. *J. Atmos. Sci.*, **51**, 711–728.

Sui, C.-H., X. Li, and K.-M. Lau, 1998: Radiative-convective processes in simulated diurnal variations of tropical oceanic convection. *J. Atmos. Sci.*, **55**, 2345–2359.

Sui, C.-H., X. Li, M.-J. Yang, and H.-L. Huang, 2005: Estimation of oceanic precipitation efficiency in cloud models. *J. Atmos. Sci.*, **62**, 4358–4370.

Sui, C.-H., X. Li, and M.-J. Yang, 2007: On the definition of precipitation efficiency. *J. Atmos. Sci.*, **64**, 4506–4513.

Tao, W.-K., 2003: Goddard Cumulus Ensemble (GCE) model: Application for understanding precipitation processes. AMS Meteorological Monographs—Cloud Systems, Hurricanes and TRMM, 107–138.

Tao, W.-K., and S.-T. Soong, 1986: The study of the response of deep tropical clouds to mesoscale processes: Three-dimensional numerical experiments. *J. Atmos. Sci.*, **43**, 2653–2676.

Tao, W.-K., and J. Simpson, 1989: Modeling study of a tropical squall-type convective line. *J. Atmos. Sci.*, **46**, 177–202.

Tao, W.-K., and J. Simpson, 1993: The Goddard Cumulus Ensemble model. Part I: Model description. *Terr. Atmos. Oceanic Sci.*, **4**, 35–72.

Tao, W.-K., J. Simpson, and S.-T. Soong, 1987: Statistical properties of a cloud ensemble: A numerical study. *J. Atmos. Sci.*, **44**, 3175–3187.

Tao, W.-K, J. Simpson, and M. McCumber, 1989: An ice-water saturation adjustment. *Mon. Wea. Rev.*, **117**, 231–235.

Tao, W.-K., J. Simpson, C.-H. Sui, B. Ferrier, S. Lang, J. Scala, M.-D. Chou, and K. Pickering, 1993: Heating, moisture and water budgets of tropical and midlatitude squall lines: Comparisons and sensitivity to longwave radiation. *J. Atmos. Sci.*, **50**, 673–690.

Tao, W.-K., S. Lang, J. Simpson, W. S. Olson, D. Johnson, B. Ferrier, C. Kummerow, and R. Adler, 2000: Vertical profiles of latent heat release and their retrieval for TOGA COARE convective systems using a cloud resolving model, SSM/I, and ship-borne radar data. *J. Meteor. Soc. Japan*, **78**, 333–355.

Tao, W.-K., C.-L. Shie, J. Simpson, S. Braun, R. H. Johnson, and P. E. Ciesielski, 2003: Convective systems over the South China Sea: Cloud resolving model simulations. *J. Atmos. Sci.*, **60**, 2929–2955.

Tao, W.-K., C.-L. Shie, D. Johnson, and J. Simpson, 2004: Surface energy budget and precipitation efficiently for convective systems developed during TOGA COARE, GATE, SCSMEX and ARM: Cloud-resolving model simulations. *J. Atmos. Sci.*, **61**, 2405–2423.

Tompkins, A. M., 2000: The impact of dimensionality on long-term cloud-resolving model simulations. *Mon. Wea. Rev.*, **128**, 1521–1535.

Tuleya, R. E., and Y. Kurihara, 1978: A numerical simulation of the landfall of tropical cyclones. *J. Atmos. Sci.*, **35**, 242–257.

Wang, J.-J., X. Li, and L. Carey, 2007: Evolution, structure, cloud microphysical and surface rainfall processes of a monsoon convection during the South China Sea Monsoon Experiment. *J. Atmos. Sci.*, **64**, 360–380.

Wu, X., W. W. Grabowski, and M. W. Moncrieff, 1998: Long-term evolution of cloud systems in TOGA COARE and their interactions with radiative and surface processes. Part I: Two-dimensional cloud-resolving model. *J. Atmos. Sci.*, **55**, 2693–2714.

Xu, K.-M., 1995: Partitioning mass, heat, and moisture budgets of explicitly simulated cumulus ensembles into convective and stratiform components. *J. Atmos. Sci.*, **52**, 551–573.

Xu, K.-M., and D. A. Randall, 1996: Explicit simulation of cumulus ensembles with the GATE Phase III data: Comparison with observations. *J. Atmos. Sci.*, **53**, 3710–3736.

Xu, K.-M., and Coauthors, 2002: An intercomparison of cloud resolving models with the atmospheric radiation measurement summer 1997 Intensive Observation Period data. *Quart. J. Roy. Meteor. Soc.*, **128**, 593–624.

Xu, X., F. Xu, and B. Li, 2007: A cloud-resolving modeling study of a torrential rainfall event over China. *J. Geophys. Res.*, **112**, D17204, doi: 10.1029/2006JD008275.

Yue, C., 2009: Quantitative analysis of torrential rainfall associated with typhoon landfall: A case study of Typhoon Haitang (2005). *Progress in Natural Science*, **19**, 55–63.